Heat transfer analysis and numerical simulation of a parabolic trough solar collector

A.A. Hachicha, I. Rodríguez, R. Capdevila, A. Oliva*

[a] *Centre Tecnològic de Transferència de Calor, Universitat Politècnica de Catalunya,ETSEIAT, Colom 11, 08222 Terrassa (Barcelona), Spain.*

Abstract

Parabolic trough solar collector is the most proven industry-scale solar generation technology today available. The thermal performance of such devices is of major interest for optimising the solar field output and increase the efficiency of power plants. In this paper, a detailed numerical heat transfer model based on the finite volume method for these equipment is presented. In the model, the different elements of the receiver are discretised into several segments in both axial and azimuthal directions and energy balances are applied for each control volume. An optical model is also developed for calculating the non-uniform solar flux distribution around the receiver. This model is based on finite volume method and ray trace techniques and takes into account the finite size of the Sun. The solar heat flux is determined as a pre-processing task and coupled to the energy balance model as a boundary condition for the outer surface of the receiver. The set of algebraic equations are solved simultaneously using direct solvers. The model is thoroughly val-

*Tel: +34 93 739 8192; fax: +34 93 739 8101
Email address: cttc@cttc.upc.edu (A. Oliva)
URL: http://wwww.cttc.upc.edu (A. Oliva)

idated with results from the literature. First, the optical model is compared with known analytical solutions. After that, the performance of the overall model is tested against experimental measurements from Sandia National Laboratories and other un-irradiated receivers experiments. In all cases, results obtained shown a good agreement with experimental and analytical results.
Keywords: Parabolic trough, CSP, numerical model, heat transfer analysis, Optical model

---

Nomenclature

Greek Letters

α absorptance factor

β thermal expansion coefficient $[1/K]$

δ molecular diameter $[m]$

ϵ emittance

η efficiency

γ intercept factor

κ absorption coefficient

μ dynamic viscosity $[kg/ms]$

ν kinematic viscosity $[m^2/s]$

Φ scattering phase function

ϕ rim angle

ϕ_s finite size of the Sun

ρ density $[kg/m^3]$

ρ_s specular reflectance

σ Stefan-Boltzmann constant $5.67 \times 10^{-8}[W/m^2K^4]$

σ_s scattering coefficient

τ transmittance

θ circumferential direction

φ angle between the reflected ray and the x axis

ξ thermal diffusivity$[m^2/s]$

Roman Letters

A area $[m^2]$

C_p specific heat at constant pressure $[J/kgK]$

D diameter $[m]$

e thickness of the tube $[m]$

f focal distance of the parabola

F view factor

g gravity$[m/s^2]$

h convective heat transfer coefficient $[W/m^2K]$

GC geometric concentration

$\hbar$ enthalpy [J/kg]

H irradiation$[W/m^2]$

i incident direction

I irradiation per unit length $[W/m]$

I_b Planck black body intensity $[W/m^2]$

J radiosity $[W/m^2]$

k thermal conductivity $[W/mK]$

$\dot{m}$ mass flow rate $[kg/s]$

n normal direction to the reflector surface

N number of control volumes

Nu Nusselt number (hD/k)

P pressure $[Pa]$

Pr Prandtl number $(\mu C_p/k)$

$\dot{q}$ net heat flux per unit of length $[W/m]$

$\dot{Q}$ power $[W]$

r reflected direction

Ra Rayleigh number $(g\beta\Delta T D^3/(\nu\xi)$

Re Reynolds number $(\rho v D/\mu)$

s distance traveled by a ray $[m]$

t time$[s]$

T temperature $[K]$

v velocity$[m/s]$

V volume $[m^3]$

W aperture $[m]$

$\dot{\mathrm{W}}$ work $[W]$

Subscripts

a absorber

an annular region

c collector

$cond$ conduction

$conv$ convection

e environment

eff effective

ex exterior

f fluid

g glass envelope

in input, Inner

inc incident

opt optical

out output

ref reflected

s sky

$s.inc$ solar incident

$s.rad$ solar radiation

$t.rad$ thermal radiation

th thermal

u useful

z longitudinal direction

1. Introduction

Concentrated solar power plants are one of the most promising and mature renewable options for electric generation. Parabolic trough collectors (PTC) are the most proven, widespread and commercially tested technology available for solar harnessing. The majority of the parabolic trough plants deployed operate at temperatures up to 400 °C using synthetic oil as heat

transfer fluid (HTF) [1]. A PTC is constructed as a long parabolic mirror with a dewar tube running its length in the focal line (see Figure 1). The HTF rcirculates through the tube and absorbs the concentrated sunlight. The surface of the absorber is covered with a selective coating which has a high absorptance for solar radiation and low emittance for thermal radiation. A glass envelope is used around the absorber tube to reduce the convective heat losses with vacuum in the space between the absorber and the glass cover. The PTC is aligned to the north-south axis and tracks the Sun from east to west as it moves across the sky using a tracking mechanism system.

Many works have been carried out to study the heat transfer process in PTC without taking into account the non-uniformity of the solar radiation and heat losses along the cross-section of the absorber tube. Dudley et al. [2] performed tests at Sandia National Laboratories to determine the thermal losses and thermal efficiency of the PTC used in LS2 Solar Thermal Electric Generation Systems (SEGS). They also proposed a one-dimensional (1D) model to analyse the thermal behaviour and performance of the LS2 SEGS collector assuming a uniform absorber temperature and neglecting the solar absorption in the envelope and all conduction effects. Foristall [3] implemented both a 1D and a two-dimensional model (2D) by dividing the absorber into several segments. They analysed the thermal behaviour of a PTC but considered a uniform solar flux and neglected the thermal radiation influence from the collector. A direct steam generation (DSG) collector model was proposed by Odeh et al. [4] based on the absorber wall temperature rather than the working fluid temperature. The heat losses for steam as HTF were lower than those obtained for synthetic oil. García-Valladares

and Velázquez [5] proposed a numerical simulation of the optical, thermal and fluid dynamic behaviour of a single-pass solar PTC and extended the study by replacing the absorber with a counter-flow concentric circular heat exchangers (double-pass). They neglected the non-uniform solar flux distribution and considered only the thermal radiation heat losses between the absorber tube and glass envelope for the case of vacuum in the annular space. Stuetzle [6] proposed a 2D unsteady state analysis of solar collector absorber to calculate the collector field outlet temperature: the model was solved by discretising the partial differential equations obtained by the energy balance. Padilla et al. [7] presented a 1D heat transfer model of a PTC taking into account the thermal interaction between adjacent surfaces and neglecting the non-uniformity of the solar flux.

The majority of the published studies about the heat transfer process in the PTC, calculate the heat losses and thermal performance considering the solar radiation as a constant and neglecting the realistic non-uniform solar heat flux in the azimuthal direction. Only a few authors have treated this dependence, i.e., some models for determining the optical behaviour of a PTC rely on analytical techniques and most of them use ray-tracing techniques to evaluate the optical efficiency. Jeter [8, 9] presented a mathematical formulation based on the Gaussian function to calculate the concentrated solar flux density and the optical behaviour of a PTC taking into account imperfect reflection, transmission and absorption. Güven and Bannerot [10] established an optical model which used a ray-tracing technique to evaluate the optical performance and determined the optical errors by means of a statistical analysis. He et al. [11] combined the Monte Carlo ray-tracing method (MCRT)

with a computational fluid dynamics (CFD) analysis in the HTF to simulate the coupled heat transfer problem. Their numerical results were compared with the analytical results of Jeter [8] as well as with the LS-2 solar collector test data [2] using different configurations.

In the present work, a detailed numerical simulation of the optical and thermal behaviour of a PTC is presented. A new geometrical-numerical method has been developed to simulate the solar heat flux distribution around the absorber tube. The heat collector element (HCE) is discretised into several segments in both axial and azimuthal directions using the Finite Volume Method (FVM) and an energy balance is applied for each control volume. A thermal radiation analysis is carried out between the HCE and the surrounding to calculate the radiative heat losses. The numerical model has been validated with experimental results obtained by Sandia National Laboratories [2] as well as un-irradiated receivers experiments [12] and a good agreement has been obtained. The optical model has been also verified with analytical results of Jeter [8, 9] and MCRT results of He et al. [11].

2. PTC numerical model

The general modelling approach is based on an energy balance about the HCE. It includes the direct normal solar irradiation, the optical losses from both, the parabola and the HCE, the thermal losses from the HCE, and the gains in the HTF.

During a sunny day, the incident solar radiation is reflected by the mirrors and concentrated at the HCE. A small amount of this energy is absorbed by the glass envelope $\dot{q}_{g,s.rad}$ and the remaining is transmitted and absorbed

by the absorber selective coating $\dot{q}_{a,s.rad}$. A part of the absorbed energy is transferred to the HTF by forced convection $\dot{q}_{a-f,conv}$ and the other part is returned to the glass envelope by natural convection $\dot{q}_{a-g,conv}$ and thermal radiation $\dot{q}_{a-g,t.rad}$. The energy coming from the absorber (convection and thermal radiation) pass through the glass envelope and along with the absorbed energy by the the glass envelope, is lost to the environment by convection $\dot{q}_{g-e,conv}$ and thermal radiation $\dot{q}_{g-e,t.rad}$ (see Figure 1).

In this heat transfer model, an energy balance is applied over each component of the HCE. The energy equation in its integral form can be written as

$$\dot{\mathrm{Q}} - \dot{\mathrm{W}} = \int_{cs} \left(h + \frac{v^2}{2} + gz \right) \left(\rho \overrightarrow{v} \overrightarrow{dA} \right) + \frac{\partial}{\partial t} \int_{cv} \left(u + \frac{v^2}{2} + gz \right) (\rho dV) \quad (1)$$

The FVM is used to discretise the domain and apply the energy conservation at each control volume (CV) under steady state conditions. The HCE is divided into N_z CVs in the axial direction and N_θ CVs in the azimuthal direction. The HTF is only discretised in the longitudinal direction (see figure 2 a and b).

Both, temperatures and heat fluxes, vary along the circumference and the length of the HCE except for the fluid which varies only along the length of the absorber. The energy balance equations are determined by applying equation 1 at each CV as is shown hereafter.

For an i-th HTF CV, the energy balance equation can be expressed as (see figure 2 c)

$$\dot{q}^i_{a-f,conv} = \dot{m} \left[\hbar^i_f - \hbar^{i+1}_f \right] = \dot{m} C_p \left[T^i_f - T^{i+1}_f \right] \quad (2)$$

For an absorber tube CV, the energy balance equation is given by (see figure 2 d)

$$\sum_{cv} \dot{q}^{ij} = \dot{q}_{a,cond} + \dot{q}^{ij}_{a,s.rad} - \dot{q}^{ij}_{a-g,conv} - \dot{q}^{ij}_{a-g,t.rad} - \dot{q}^{ij}_{a-f,conv} = 0 \qquad (3)$$

where

$$\dot{q}_{a,cond} = \dot{q}^{ij}_{a,cond-z} - \dot{q}^{i+1j}_{a,cond-z} + \dot{q}^{ij}_{a,cond-\theta} - \dot{q}^{ij+1}_{a,cond-\theta} \qquad (4)$$

In a similar way, the energy balance for a glass envelope tube CV can be obtained as follows (see figure 2 e)

$$\sum_{cv} \dot{q}^{ij} = \dot{q}_{g,cond} + \dot{q}^{ij}_{g-a,conv} + \dot{q}^{ij}_{g-a,t.rad} - \dot{q}^{ij}_{g-e,conv} - \dot{q}^{ij}_{g-e,t.rad} + \dot{q}^{ij}_{g-s.rad} = 0 \quad (5)$$

where

$$\dot{q}_{g,cond} = \dot{q}^{ij}_{g,cond-z} - \dot{q}^{i+1j}_{g,cond-z} + \dot{q}^{ij}_{g,cond-\theta} - \dot{q}^{ij+1}_{g,cond-\theta} \qquad (6)$$

A detailed analysis of how each of these heat fluxes are determined is given hereafter.

2.1. Convection heat transfer between the HTF and the absorber

The convection heat transfer between the HTF and the absorber metal pipe is evaluated considering the convective heat flux from each absorber CV in the azimuthal direction as,

$$\dot{q}^{i}_{a-f,conv} = \sum_{j} h_f (T^{ij}_a - T^{i}_f) \frac{\pi D_{a,in}}{N_\theta} \qquad (7)$$

where $h_f = \dfrac{Nu_{D_{a,in}} k}{D_{a,in}}$ is the HTF convection heat transfer coefficient at T_a^{ij} and is evaluated as a function of the Nusselt number $Nu_{D_{a,in}}$. Due to the lack of specific correlations in literature for evaluating the Nusselt number taking into account the temperature distribution of the absorber at each azimuthal CV, correlations for isothermal cylinders are considered. Specifically, the Gnielinski correlation [13] is used for turbulent and transitional flow ($Re > 3200$) in circular ducts, which reads,

$$Nu_{D_{a,in}} = \frac{(C/2)(Re_{D_{a,in}} - 1000)Pr}{1 + 12\sqrt{C/8}(Pr^{2/3} - 1)} \left(\frac{Pr}{Pr_w}\right)^{0.11} \tag{8}$$

with $C = (1.82log(Re_D) - 1.64)^{-2}$.

2.2. Conduction heat transfer through the absorber wall and the glass envelope

Heat conduction through the absorber wall and the glass cover is considered in the axial and azimuthal directions, whereas the heat conduction through the support brackets is neglected. The energy rate per unit length conducted across the azimuthal direction of a cylinder is defined as

$$\dot{q}_{cond-\theta} = -\frac{d(kT)}{rd\theta} e \tag{9}$$

where in the above expression e represents the thickness of either the absorber or glass envelope tube. In a similar manner, for the axial direction the conduction heat flux is defined as

$$\dot{q}_{cond-z} = -\frac{d(kT)}{dz} A_z \tag{10}$$

where A_z is the cross-section area of the CV. Both equations (9 and 10) are applied to the absorber and the glass envelope tubes taking into account the conductivity as a function of temperature of both materials.

2.3. Convection heat transfer between the absorber and the glass envelope

When the annular region is assumed as a perfect vacuum, the convection heat transfer can be ignored in the energy balance. However, in operational solar plants the vacuum condition in the annulus can change due to broken seals, hydrogen penetration and getter decomposition . In the present model, convection heat transfer $\dot{q}^{ij}_{a-g,conv}$ is calculated as follows,

$$\dot{q}^{ij}_{a-g,conv} = \ h_{an}(T^{ij}_a - T^{ij}_g)\frac{\pi D_{a,ex}}{N_\theta} \tag{11}$$

where h_{an} is calculated depending on free molecular convection or natural convection takes place.

When the HCE is under vacuum at low pressure ($P \simeq 0.013Pa$), free molecular convection occurs. The heat transfer coefficient is then evaluated as [14],

$$h_{an} = \frac{k_{std}}{[(D_{g,in}/2)ln(D_{g,in}/D_{a,ex}) + b\lambda(D_{a,ex}/D_{g,in} + 1)]} \tag{12}$$

$$b = \frac{(2-a)(9\gamma - 5)}{2a(\omega + 1)} \tag{13}$$

$$\lambda = \frac{2.331 \times 10^{-20} T^{ij}_{a-g}}{P_a \delta^2} \tag{14}$$

where k_{std} is the thermal conductivity of the annulus gas at standard temperature and pressure, b the interaction coefficient, λ the mean-free path between collisions of a molecule, a the accommodation coefficient, ω the ratio of specific heat for the annulus gas, T^{ij}_{a-g} the average temperature of the gas in the annulus $(T^{ij}_a + T^{ij}_g)/2$, P_a the annulus gas pressure and δ molecular diameter of the gas (air and hydrogen have molecular diameters of 3.53×10^{-8} and 2.32×10^{-8}, respectively). The accommodation coefficient a depends on, either the gas surface arrangement or the level of contaminant gas layer absorbed on the surface and, varies between 0.01 to unity according to experimental studies [15]. In this study, the surface is assumed well cleaned and the accommodation coefficient is then fixed to one.

When the vacuum is lost, natural convection within the annulus occurs. The heat transfer coefficient is then expressed with the Raithby and Holland's correlation [16] for natural convection in an annular space between horizontal cylinders,

$$h_{an} = \frac{2k_{eff}}{D_{a,ex} ln(D_{g,in}/D_{a,ex})} \tag{15}$$

$$k_{eff} = k(0.386) \left[\frac{Pr}{0.861 + Pr}\right]^{0.25} (Ra_c)^{0.25} \tag{16}$$

$$Ra_c = \frac{ln(D_{g,in}/D_{a,ex})^4}{L^3 \left(D^{-0.6}_{a,ex} + D^{-0.6}_{g,in}\right)^5} Ra_L \tag{17}$$

being the effective thermal conductivity k_{eff} function of the thermophysical properties of the gas and the equivalent Rayleigh number Ra_c. This correlation is used for the range of $(10^2 \leq Ra_c \leq 10^7)$ and Ra_L is evaluated at the air gap distance $(D_{g,in} - D_{a,ex})/2$.

2.4. Thermal radiation heat transfer between the absorber and the glass envelope

The surfaces of the absorber and glass envelope are considered as grey and diffuse emitters and reflectors. The glass envelope is assumed to be opaque to the thermal radiation. The net radiation method [17] is applied to the cross section of the HCE in order to calculate $\dot{q}_{a-g,t.rad}$ as well as $\dot{q}_{g-a,t.rad}$ (equations 3 and 5). The effect of the axial direction is neglected. The Hottel's crossed-string method [17] is used for calculating the view factors by connecting the faces of each tube and making sure that no visual obstruction remains between them.

In what follows, F_{ki}^{mn} is the view factor or shape factor from the surface of CV k at the material m to the surface of CV i at the material n. Since the absorber surface is convex, the view factor between any two CVs of the absorber tube is zero, $F_{ki}^{aa} = 0$. On the contrary, the view factors for the glass envelope, F_{ki}^{gg} are not null. They are calculated, all together with the view factors between the absorber and the glass envelope (F_{ki}^{ag} and F_{ki}^{ga}), using also the crossed-string method.

The thermal radiative heat flux leaving the j-th absorber CV is expressed by

$$\begin{aligned} \dot{q}_{a-g,t.rad}^{ij} &= \dot{q}_{a,t.rad}^{j} = (J_a^j - H_a^j) = \epsilon_a \left[\sigma {T_a^j}^4 - H_a^j\right] \\ &= \epsilon_a \left[\sigma {T_a^j}^4 - \sum_l (F_{jl}^{ag} J_g^l)\right] \end{aligned} \tag{18}$$

The thermal radiation gained by a glass envelope CV j is given by

$$\begin{aligned} \dot{q}^{ij}_{g-a,t.rad} &= \dot{q}^{j}_{g,t.rad} = (J^j_g - H^j_g) = \epsilon_g \left[\sigma {T^j_g}^4 - H^j_g\right] \\ &= \epsilon_g \left[\sigma {T^j_g}^4 - \sum_k (F^{ga}_{jk} J^k_a) - \sum_r (F^{gg}_{jr} J^r_g)\right] \end{aligned} \tag{19}$$

The total thermal radiative energy leaving the absorber tube is calculated by integrating the radiative heat flux around the absorber.

$$\dot{q}_{a-g,t.rad} = \sum_j^{N_\theta} \dot{q}^j_{a,t.rad} \tag{20}$$

In a similar way, the total thermal radiative energy gained by the glass envelope is calculated as

$$\dot{q}_{g-a,t.rad} = \sum_j^{N_\theta} \dot{q}^j_{g,t.rad} \tag{21}$$

2.5. Convection heat transfer from the glass envelope to the environment

The convection heat transfer from the glass envelope to the ambient is computed as

$$\dot{q}^{ij}_{g-e,conv} = h_e (T^{ij}_g - T_{amb}) \frac{\pi D_{g,ex}}{N_\theta} \tag{22}$$

The heat transfer coefficient, h_e, is evaluated depending on whether the convection is natural or forced. There are many correlations for predicting convection heat transfer from horizontal pipes under both, natural and forced conditions. After comparing different empirical correlations presented in the technical literature, the ones indicated hereafter are selected as they work

better for the conditions under study. Thus, for natural convection the correlation developed by Churchill and Chu [18] for horizontal cylinders for the calculation of the average Nusselt number is recommended.

$$Nu_{D_{g,ex}} = \left[0.6 + 0.387 \left(\frac{Ra_{D_{g,ex}}}{\left(1 + (0.559/Pr)^{9/16}\right)^{16/9}} \right)^{1/6} \right]^2 \tag{23}$$

If the PTC is supposed to work exposed to wind conditions, i.e., under forced convection, then the convection heat transfer coefficient is determined using the correlation of Churchill and Bernstein [19] for a cylinder in cross flow. This equation is recommended to be used for all $Re_{D_{g,ex}} Pr > 0.2$.

$$Nu_{D_{g,ex}} = 0.3 + \frac{0.62 Re_{D_{g,ex}}^{0.5} Pr^{1/3}}{\left[1 + (0.4/Pr)^{2/3}\right]^{1/4}} \left[1 + \left(\frac{Re_{D_{g,ex}}}{282000} \right)^{5/8} \right]^{4/5} \tag{24}$$

2.6. Thermal radiation heat transfer between the glass envelope and the surrounding

The glass envelope is surrounded by either the collector parabola and the sky. Thus, thermal radiation heat transfer must consider the radiation exchange with both. In the present model, the glass envelope is assumed to be a small convex grey object and the sky as a large black body cavity ($\epsilon_s = 1$) at temperature T_s. The collector parabola surface is considered diffuse and opaque to the thermal radiation. The view factors are determined using the crossed-string method, similar to the treatment in section 2.4.

$$\dot{q}^{ij}_{g-e,t.rad} = \dot{q}^{j}_{g,t.rad} = (J^i_g - H^i_g) = \epsilon_g[\sigma {T^i_g}^4 - H^i_g] = \epsilon_g \left[\sigma {T^i_g}^4 - \sum_k (F^{gc}_k J_c + F^{gs}_k J_s)\right] \quad (25)$$

where $j_c = \epsilon_c \sigma T_c^4$ and $J_s = \sigma T_s^4$. The thermal radiative heat energy lost to the environment is then calculated by integrating the radiative flux around the glass envelope.

$$\dot{q}_{g-e,t.rad} = \sum_j^{N_\theta} \dot{q}^{j}_{g,t.rad} \quad (26)$$

2.7. Solar irradiation absorption

An optical model is developed to calculate the solar heat flux around the HCE. This model uses a numerical-geometrical method based on ray trace and FVM techniques to project the solar optic cone of so known the finite size of the Sun [20] on the absorber surface.

The incident solar irradiation is represented as a ray package, defined by the optic cone or *sunshape*, i.e., rays are symmetrically distributed around a central one within the angle range $(\phi_s, -\phi_s)$, where $\phi_s = 16$ arcminutes [21]. The solar-optical properties of the system (specular reflectance of the collector parabola, ρ_s, the effective glass envelope transmittance, τ_{eff}, and the effective coating absorptance of the absorber, α_{eff}) are assumed to be independent of the temperature and the angle. It is considered that the thickness of the glass is very small, so the change of direction of the rays that cross the glass according to the Snell's law is neglected. Thus, the present method computes directly the solar irradiation that reaches the absorber

tube. The effect of the glass is considered by means of reducing the solar irradiation that arrives at the absorber tube by τ_{eff}.

The method consists on resolving the Radiative Transfer Equation (RTE). For a general absorbing, emitting and scattering medium at the position x, y and the direction $\hat{s}$, the RTE may be written as,

$$\begin{aligned} \frac{dI(x,y,\hat{s})}{ds} &= \kappa(x,y)I_b(x,y) - (\kappa(x,y)+\sigma_s(x,y))I(x,y,\hat{s}) \\ &+ \frac{\sigma_s(x,y)}{4\pi}\int_{4\pi} I(x,y,\hat{s}')\Phi(\hat{s}',\hat{s})d\Omega' \end{aligned} \tag{27}$$

where $I(x,y,\hat{s})$ is the radiative intensity at the position (x,y) and in the direction $\hat{s}$, $\kappa(x,y)$ and $\sigma_s(x,y)$ are the absorption and scattering coefficients, respectively. $\Phi(\hat{s}',\hat{s})$ is the scattering phase function and I_b is the Planck black body intensity. In the present work, the medium is assumed transparent so that $\kappa(x,y)=0$ and $\sigma_s(x,y)=0$ leading to,

$$\frac{dI(x,y,\hat{s})}{ds} = 0 \tag{28}$$

Because of the symmetry of the problem, the treatment is described for one half of the PTC and is the same for the other part. The PTC is discretised into four grid systems as shown in Figure 3: *i)* N_1: the number of CVs in the space between the absorber and the edge of the aperture, *ii)* N_2: the number of CVs in the front space of the absorber tube, where it receives only the direct irradiation from the Sun, *iii)* N_3: the number of CVs around the absorber tube in the azimuthal direction and, *iv)* N_4 the total number of the control angles in the optic cone.

First, the incident optic cone is symmetrically discretised into N_4 control angles around the central ray and projected on the parabola surface, represented by N_1 CVs, and on the front face of the absorber, represented by N_2 CVs. The direct incident solar irradiation, i.e., solar irradiation that reaches the absorber surface, without reflection on the parabola, is integrated directly over each absorber CV. The other part of the incident solar irradiation, hits the parabola surface and is then specularly reflected. The incident ray in the direction $\vec{i}$ is reflected respect to the normal of reflector surface $\vec{n}$ (see Figure 3). The direction $\vec{r}$ of the reflected ray is given by the law of specular reflection,

$$\vec{r} = \vec{i} - 2(\vec{n} \cdot \vec{i})\vec{n} \tag{29}$$

Since perfect solar elevation tracking system is considered, the reflected rays are concentrated in the focus line of the parabola. The amount of solar energy transported by a reflected ray q_{ref} is given by,

$$q_{ref} = \frac{\rho_s I_{s.in} \Delta_w}{N_4} \tag{30}$$

where $\Delta_w = \left(\frac{\frac{W}{2} - r_a}{N_1}\right)$ is the length of the CV in the aperture zone represented by N_1 CVs.

For a given CV of the aperture zone, the reflected central ray, which is coming from the central ray of the optic cone, makes an angle $\varphi_c = \tan^{-1}(\frac{f-y}{x})$ with the x axis, where x and y define the spatial position of the intersection point of the ray at the parabola (see Figure 4). The angle φ formed by a general reflected ray that impinges in a given CV of the aperture zone, and the x axis for each coming ray from the optic cone is then

calculated as $\varphi_m = \varphi_c \pm m\Delta\varphi$ where m is an integer that varies from 0 to $N_4/2$. After that, the absorber tube is looped to determine the intercepted rays coming from the reflected rays of the optic cone. For an absorber CV j, φ_1 and φ_2 are defined (see Figure 4).

$$\varphi_1 = \tan^{-1}\left[\frac{|f-y| - r_a\cos\theta_j}{|x - r_a\sin\theta_j|}\right] \tag{31}$$

$$\varphi_2 = \tan^{-1}\left[\frac{|f-y| - r_a\cos\theta_{j+1}}{|x - r_a\sin\theta_{j+1}|}\right] \tag{32}$$

A reflected ray which forms an angle φ with the x axis is intercepted by j-th absorber CV if φ lays between φ_1 and φ_2. This procedure is repeated for all CVs of the aperture zone N_1. The solar energy absorbed by the absorber tube and the glass envelope is obtained by summing the reflected rays (q_{ref}) that reach the j-th CV.

$$\dot{q}^j_{a,s.rad} = (\tau\alpha)_{eff}\sum q_{ref} \tag{33}$$

$$\dot{q}^j_{g,s.rad} = (1-(\tau\alpha)_{eff})\sum q_{ref} \tag{34}$$

The total absorbed energy $\dot{q}_{a,s.rad}$ is determined by adding the direct (that lies in N_2) and the reflected incident solar irradiation, which corresponds to the integral of equation (33), over all CVs of the absorber (N_3).

The optical model provides the solar heat flux distribution around the HCE, as well as, the optical efficiency η_{opt} of the PTC, which is defined as the ratio of energy absorbed by the absorber to the energy incident on the collector's aperture.

$$\eta_{opt} = \frac{\dot{q}_{a,s.rad}}{\dot{q}_{s.inc}} = \frac{\left((W - D_a)\rho_s + D_a\right)(\tau\alpha)_{eff}}{W} \tag{35}$$

This ratio is often approximated to $\rho_s(\tau\alpha)_{eff}$ as the reflected part is much more important than the direct one.

The previous treatment have dealt with PTC having a perfect parabolic cross-sections. However, such perfection is never attained in practice. In fact, the concentration is degraded due to imperfections or errors that may result from poor manufacturing and/or assembly, imperfect tracking of the Sun, and/or poor operating conditions. These optical errors are included in the so-called intercept factor γ which is usually calculated using statistical approaches [10, 22] or experimentally [23] and remains only an approximation.

Using a solar elevation tracking system, the Sun will be maintained in the $y-z$ plane but not usually normal to the collector aperture ($x-z$ plane) making an incident angle φ_{inc} respect to the normal. Then, the reflected energy q_{ref} is decreased by $\cos(\varphi_{inc})$ while the apparent cone optic is expanded and increased as $1/\cos(\varphi_{inc})$. Thus, the algorithm of solar absorption analysis for non-zero incident solar irradiation remains the same as described before with both modifications of the reflected energy and cone optic size. It should be pointed out that, the implementation and the resolution of this optical model is much faster than other ray tracing techniques and requires lower computational efforts for obtaining similar results.

3. Numerical Solution

As commented in the previous section, the numerical analysis is carried out by using the FVM under steady state conditions. For the fluid inside the

absorber, a single phase (liquid) incompressible flow is assumed. The energy balance equations (equations 2, 3 and 5) result in a set of non-linear algebraic equations where temperatures and heat fluxes are coupled and solved using an iterative procedure. The solar radiative heat flux (equations 33 and 34) is determined as a pre-processing task. This flux is added to the balance energy model as a boundary condition for the outer surface of the absorber/glass tube by assuming the solar absorption as surface phenomenon because of the small thickness of the surface layer over which absorption is taking place [17].

For a HTF control volume, the temperature values are obtained from the 1D discretised equations by using the known values at the inlet section and the wall boundary conditions. A high-order numerical scheme (SMART) [24] is used to calculate the temperature at the faces of the CVs. The set of algebraic equations are then solved by a direct solver (TDMA) in the longitudinal tube direction.

For the absorber tube and the glass envelope, a central difference scheme is used in the discretisation process. The linear algebraic equations obtained from the discretisation of the governing equations in the absorber and the glass envelope are implemented with the corresponding boundary conditions and then solved using a direct solver based on LU decomposition.

The general algorithm, as can be seen in Figure 5, is divided in two steps: the pre-processing calculation of the concentrated solar flux distribution (the optical model) and the thermal model for resolving the energy balance at the HCE. The energy balance model provides the temperature distribution in the HCE as well as the performance of a PTC by calculating the useful energy, the thermal losses and the thermal efficiency. The PTC thermal efficiency is

determined as,

$$\eta_{th} = \frac{q_u}{A_w I_{s.inc}} \tag{36}$$

The useful energy is obtained by summing the heat gained by the HTF along the absorber. Thus,

$$q_u = \sum_{i}^{N_z} \sum_{j}^{N_\theta} \dot{q}^{ij}_{a-f,conv} \tag{37}$$

The heat losses are the sum of the convective and the thermal radiative flux lost by the absorber tube.

$$q_{heat\,loss} = \sum_{i}^{N_z} \sum_{j}^{N_\theta} (\dot{q}^{ij}_{a-g,conv} - \dot{q}^{ij}_{a-g,rad}) \tag{38}$$

4. Computational results and validation

The validation of the model is carried out in two steps: the validation of the optical model and then, the validation of the thermal and overall model.

4.1. Optical model validation

In order to verify the accuracy of the optical model, the results are compared with available references from the literature. The geometrical-numerical method presented in this work is validated using the ideal PTC with round absorber adopted by Jeter [9], where geometric concentration GC=20, rim angle ϕ=90° for an optic cone of 0.0075 rad and optical properties (ρ_s,τ and α) are equal to unity. Under these conditions, the solar heat flux distribution is compared to the analytical results found by Jeter

[9]. A grid independence study is carried out and tested for different grid systems. The grid with parameters N_1=640, N_2=160, N_3=160, and N_4=320 is regarded as grid-independent since there is no significant difference with the finer one. The Local Concentration Ratio (LCR), which is defined by the ratio of solar radiative heat flux falling on the surface of the absorber tube to that which falls on the reflective surface of the collector, is calculated. It is a significant parameter of the heat flux distribution. The present results are in a good agreement with those of Jeter with the same trend and the same minimum and maximum values (see Figure 6).

According to the distribution of the LCR, it can be divided in four zones: *i)* the direct radiation zone, where the absorber tube only receives the direct solar irradiation without concentration ($LCR \simeq 1$), which corresponds to N_2 zone of Figure 3, *ii)* the heat flux increasing zone, where the heat flux increases rapidly because of the reflection of the solar irradiation, *iii)* the heat flux decreasing zone, where the reflected solar flux decreases because of the parabolic shape and, *iv)* the shadow effect zone, where the heat flux is much lower and decreases rapidly because of the Sun irradiation is shadowed by the absorber tube.

In figure 6, the results obtained by He et al. [11] for the same case using a MCRT method are also plotted. As can be seen from the figure, the present model yields better results than those presented in [11] especially for the shadow effect zone.

The solar heat flux distribution around the HCE is also simulated for the same PTC described above (Jeter case) and for different incident angles. Figure 7 shows the comparison between the computed results obtained by the

present optical model and the analytical results of Jeter [9]. There is a good agreement between both results for different incident angles which proves the accuracy of the present optical model. It can also be seen from Figure 7 that the heat flux distribution decreases with the increase of the incidence angle ϕ_{inc}. This decrease is due to the effect of the cosine of the incident angle which becomes significant for larger angles (near to 90°). The optical efficiency is at maximum only when the incoming radiation is normal to the aperture. The peak of concentration is approached to the lowest position of the absorber tube (θ=180°) as the incident angle increases. The concentration tends to spread around the lower half of the absorber tube with the increasing of the incident angle.

Finally, the heat flux distribution around the absorber tube is compared with the MCRT results of He et al. [11] for the case of LS-2 solar collector [2] with an incident solar irradiation of $933.7 W/m^2$. The detailed specifications of a LS-2 solar collector are given in Table 1. Figure 8 shows the comparison of the solar heat flux distribution with the MCRT results and demonstrates a good agreement with some differences in the shadow effect zone, which have been discussed before.

Table 1: Parameter of the LS-2 solar collector [2] used in the model validation

Receiver length (L)	7.8m
Collector aperture (W)	5m
Focal distance (f)	1.84m
Absorber internal diameter ($D_{a,in}$)	0.066m
Absorber external diameter ($D_{a,ex}$)	0.070m
Glass internal diameter ($D_{g,in}$)	0.109m
Glass external diameter ($D_{g,ex}$)	0.115m
Receiver absorptance (α)	0.96
Glass transmittance (τ)	0.95
Parabola specular reflectance (ρ_s)	0.93
Incident angle (φ_{inc})	0.0

Table 2: Experimental conditions data from [2] used in the thermal model validation

Selective coatings	Cermet- Black chrome
Incident solar irradiation	755 - 982.3 W/m^2
Wind Speed	0.0 - 5.5 m/s
Flow rate	(7.95 - 9.46) $\times 10^{-4} m^3/s$
Air Temperature	267.95 - 304.85 K
Input Temperature	317.85 - 649.75 K

4.2. Thermal model validation

The thermal model is validated by comparing the results with experimental measurements obtained by Sandia National Laboratories for a collector assembly (LS-2) placed in the AZTRAK rotating platform [2]. The comparisons are carried out under different working conditions which are summarised in table 2 for a silicone HTF (syltherm 800).

In the numerical model, different numbers of longitudinal control volumes are tested to get a grid-independent solution. The grid $N_z \times N_\theta = 60 \times 60$, is considered as grid-independent since there is no significant difference in the results for finer discretisations.

Comparisons are performed for irradiated and un-irradiated absorbers and two scenarios of the annulus: *i)* vacuum and *ii)* air between the absorber and the glass envelope. The experimental tests reported at zero incident angle are used for the comparison in this paper.

The comparison of the performance against the experimental data is shown in Figures (9-11). The results for the thermal losses and the ther-

mal efficiency of the PTC follow the same trends of the experiments and the agreement here is good. The results are within the experimental uncertainty.

As it was expected, heat losses increase with the fluid temperature due to the convection, conduction, and thermal radiation losses in the annulus for both cases (air and vacuum), which cause the drop of efficiency. Moreover, the heat losses increase and the efficiency of the collector is degraded when allowing air into annulus, as well as for the use of black chrome coating, which has worse radiative properties (high emittance) than the cermet coating.

The discrepancies between the present results and the experimental measurements seem to increase with the temperature of the HTF. This can be explained by the optical properties of the HCE, which are based at lower temperatures. In addition, other unaccounted optical effects during the test operating [3], such as HCE and mirror alignment, aberration in mirrors and tracking system errors are also causes of the discrepancies. Another source of errors might be the empirical correlations used for the heat transfer coefficients. In the present work, correlations for a cylinder in cross-flow are used, but when the PTC works under wind conditions, the presence of the parabolic mirror affects the heat transfer around the HCE [25, 26]. Further work is required for obtaining appropriate correlations for such situations.

The numerical model is also validated with more recent experimental measurements of heat losses which are performed in un-irradiated absorbers [12, 27]. The experiments are done indoors using a HCE with the same dimensions as in table 1, an ambient temperature of about 296K and the flow rate is changed to obtain the desired absorber temperature. The advantage of this validation is that these experiments are performed inside the laboratory

under controlled ambient which can affect the convection heat transfer with environment as well as the optical errors in the PTC.

In these simulations, the thermal emittance of UVAC3 [12] is used. Although, in the experimental measurements of PTR70 [27] the emittance was different from UVAC3 [12], these results are also plotted just as a reference to illustrate the trend. Figure 12(a) shows the heat losses from un-irradiated absorbers and the comparison with both experimental measurements. It can be seen from the figure, that the present model reproduces the behaviour of UVAC3 HCE reasonably well and follow the same trend of PTR70 HCE. The heat losses in un-irradiated absorbers are dominated by thermal radiation and the heat transfer coefficient to the environment corresponds to natural convection (no winds). As can be seen, the current model accurately predicts heat losses and gives better agreement than the previous heat losses validation with Sandia experiments [2]. Figure 12(b) shows the variation of the glass temperature respect to the absorber temperature and the comparison with experimental tests. The main reason of the difference encountered in glass temperature is due to the variation of the optical properties with temperature as well as the effect of anti-reflective coating applied to the glass which is not included in the present model. A possible under-prediction of the convection heat transfer coefficient may be the cause of the over-prediction of the glass temperature at high operating temperature.

Finally, the case of Dudley et al. [2] ($I_b = 933.7 W/m^2$, $\dot{m} = 0.68\ kgs^{-1}$, $T_{air} = 294.35\ K$ and $T_{in} = 375.35\ K$) has been tested. The results of the thermal behaviour around the circumference of the HCE are presented in Figures (13-14). The temperature profile of both absorber and glass envelope

follows the non-uniform solar heat flux distribution which indicates that the conduction in both tubes is relatively small. The temperature of the absorber is symmetric and increases by moving along the HCE far away from the inlet. The four zones discussed in the distribution of the LCR are also present in the temperature distribution of both tubes. The temperature at the inlet of the absorber is close to the temperature of the un-irradiated absorber in the direct radiation zone where the solar flux is not concentrated.

The temperature of the absorber increases along the axial direction as shown in Figure 14 for different azimuthal positions (0°, 90° and 180°) and follows the same trend as the numerical results of Cheng et al. [28]. The absorber temperature is higher at 180° because the absorber receives more concentrated solar radiation at this angular position, while at 0° is the lowest one because there is no solar concentration in this position.

5. Conclusions

A detailed numerical model based on energy balance about the HCE for the optical and thermal analysis of PTC has been developed. A numerical-geometric method based on ray trace and FVM techniques is developed for calculating the non-uniform solar flux around the HCE. The proposed model included a detailed thermal radiative heat transfer analysis based on the crossed-string method. Different empirical correlations have been tested and selected according to the conditions under study. The optical model is validated with available analytical results from the literature, showing a quite good agreement. Once the optical model is validated, the overall thermal model is compared with the experimental measurements from Sandia Na-

tional Laboratories [2]. Results obtained matched experimental ones, although some discrepancies are observed at higher temperatures. These discrepancies might be attributed to optical properties of the HCE, other unaccounted optical effects during the test operating, and possible errors due to correlations used for the heat transfer coefficients. Further validation is carried out by comparing the results of the thermal model with experimental measurements of un-irradiated receivers. It is shown that the present model is capable of estimating reasonably well the heat losses and temperature in the HCE.

In addition to that, the overall model is tested for a given case of Dudley et al. [2] to study the thermal behaviour around the circumference of the HCE. The effect of the non-uniform incident solar radiation on the absorber tube and glass envelope was discussed. According to the results obtained, it can be concluded that the current numerical model is suitable for predicting the optical and thermal behaviour of the HCE under different operating conditions. Further work is also ongoing for determining the effect of the non uniformity solar flux distribution in the convective heat losses to the ambient and taking into account the angle attack of the wind.

Acknowledgements

This work has been partially financial supported by the "Ministerio de Economia y Competitividad, Secretaria de Estado de Investigación, Desarrollo y Innovación", Spain through projects ENE2010-17801 and UNPC 10-4E-586 (Fondos FEDER). A.A. Hachicha also wishes to thank "Agencia Española de Cooperación Internacional para el Desarrollo (AECID)" for its

support in the form of a doctoral scholarship.

References

[1] Price H, Lüpfert E, Kearney D, Zarza E, Cohen G, Gee , et al. Advances in parabolic trough solar power technology. Journal of Solar Energy Engineering 2002;124(2):109–25.

[2] Dudley V, Kolb G, Sloan M, Kearney D. SEGS LS2 solar collector-test results. Tech. Rep.; Report of Sandia National Laboratories (SANDIA-94-1884); 1994.

[3] Foristall R. Heat transfer analysis and modeling of aparabolic trough solar receiver implemented in engineering equation solver. Tech. Rep.; National Renewable Energy Laboratory(NREL); 2003.

[4] Odeh S, Morrison G, Behnia M. Modelling of parabolic trough direct steam generation solar collectors. Solar energy 1998;62(6):395–406.

[5] García-Valladares O, Velázquez N. Numerical simulation of parabolic trough solar collector: improvement using counter flow concentric circular heat exchangers. Int J Heat Mass Trans 2009;52(3-4):597–609.

[6] Stuetzle T. Automatic control of the 30 MWe SEGS IV Parabolic trough plant. Master's thesis; University of Wisconsin-Madison, College of Engineering; 2002.

[7] Padilla R, Demirkaya G, Goswami Y, Stefanakos E, Rahman M. Heat transfer analysis of parabolic trough solar receiver. Applied Energy 2011;88:5097–110.

[8] Jeter M. Analytical determination of the optical performance of parabolic trough collectors from design data. Solar Energy 1987;39(1):11–21.

[9] Jeter M. Calculation of the concentrated flux density distribution in a parabolic trough collectors by a semifinite formulation. Solar Energy 1986;37(5):335–45.

[10] Güven H, Bannerot R. Derivation of universal error parameters for comprehensive optical analysis of parabolic troughs. Journal of Solar Energy Engineering 1986;108:275–81.

[11] He YL, Xiao J, Cheng ZD, Tao YB. A MCRT and FVM coupled simulation method for energy conversion process in parabolic trough solar collector. Renewable Energy 2011;36:976–85.

[12] Burkholder F, Kutscher C. Heat-loss testing of Solel's UVAC3 parabolic trough receiver. Tech. Rep. NREL/TP-550-42394; National Renewable Energy Laboratory; 2008.

[13] Gnielinski V. New equations for heat and mass transfer in turbulent pipe and channel flow. International Chemical Engineering 1976;16(2):359–63.

[14] Ratzel A, Hickox C, Gartling D. Techniques for reducing thermal conduction and natural convection heat losses in annular receiver geometries. Journal of Heat Transfer 1979;101:108–13.

[15] Saxena S, Joshi R. Thermal Accommodation and Adsorption Coefficients of Gases (CINDAS Data Series on Material Properties). Taylor & Francis; 1989.

[16] Raithby GD, Hollands K. A general method of obtaining approximate solutions to laminar and turbulent free convection problems. Advances in Heat Transfer 1975;11:265–315.

[17] Modest M. Radiative heat transfer. Academic Press; 2003.

[18] Churchill S, Chu H. Correlating equations for laminar and turbulent free convection from a horizontal cylinder. Int J Heat Mass Trans 1975;18(9):1049–53.

[19] Churchill S, Bernstein M. A correlating equation for forced convection from gases and liquids to a circular cylinder in crossflow. Journal of Heat Transfer 1977;99(300):300–6.

[20] Riveros H, Oliva A. Graphical analysis of sun concentrating collectors. Solar Energy 1986;36(4):313–22.

[21] Evans D. On the performance of cylindrical parabolic solar concentrators with flat absorbers. Solar Energy 1977;19:379–85.

[22] Güven H, Bannerot R. Determination of error tolerances for the optical design of parabolic troughs for developing countries. Journal of Solar Energy Engineering 1986;36(6):535–51.

[23] García-Cortés S, Bello-García A, Ordóñez C. Estimating intercept factor of a parabolic solar trough collector with new supporting structure using

off-the-shelf photogrammetric equipment. Applied Energy 2012;92:815–21.

[24] Gaskell P, Lau A. Curvature compensated convective transport: SMART, a new boundeness preserving transport altgorithm. International Journal Numerical Methods Fluids 1988;8:617–41.

[25] Naeeni N, Yaghoubi M. Analysis of wind flow around a parabolic collector (1) fluid flow. Renewable Energy 2007;32(11):1898–916.

[26] Naeeni N, Yaghoubi M. Analysis of wind flow around a parabolic collector (2) fluid flow. Renewable Energy 2007;32(11):1259–72.

[27] Burkholder F, Kutscher C. Heat loss testing of Schoot's 2008 PTR70 parabolic trough receiver. Tech. Rep. NREL/TP-550-45633; National Renewable Energy Laboratory; 2009.

[28] Cheng Z, He Y, Xiao J, Tao Y, Xu R. Three-dimensional numerical study of heat transfer characteristics in the receiver tube of parabolic trough solar collector. Int Commun Heat Mass Trans 2010;37(7):782–7.

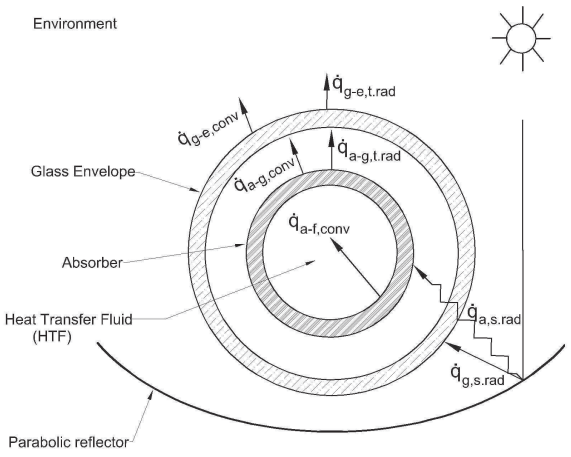

Figure 1: Heat transfer model in a cross section of the HCE (not to scale).

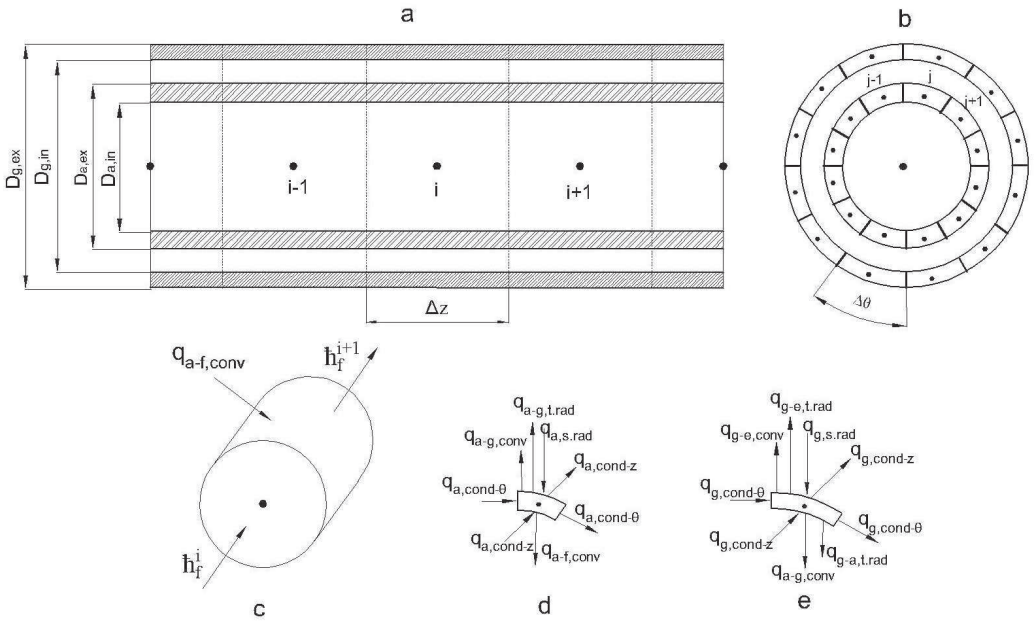

Figure 2: Longitudinal and azimuthal discretisation of the HCE: (a) longitudinal discretisation (b) azimuthal discretisation (c) HTF CV (d) absorber CV (e) glass envelope CV

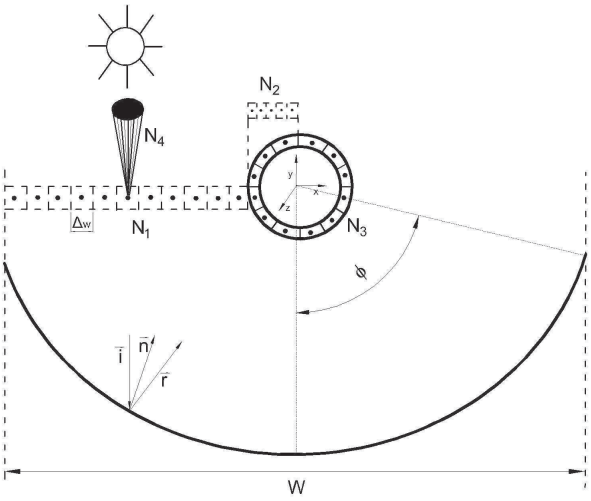

Figure 3: Schematic of spatial and angular distcretisation of the system.

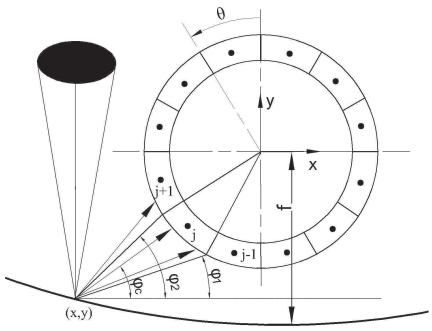

Figure 4: Schematic of the reflection of the optic cone on the absorber tube.

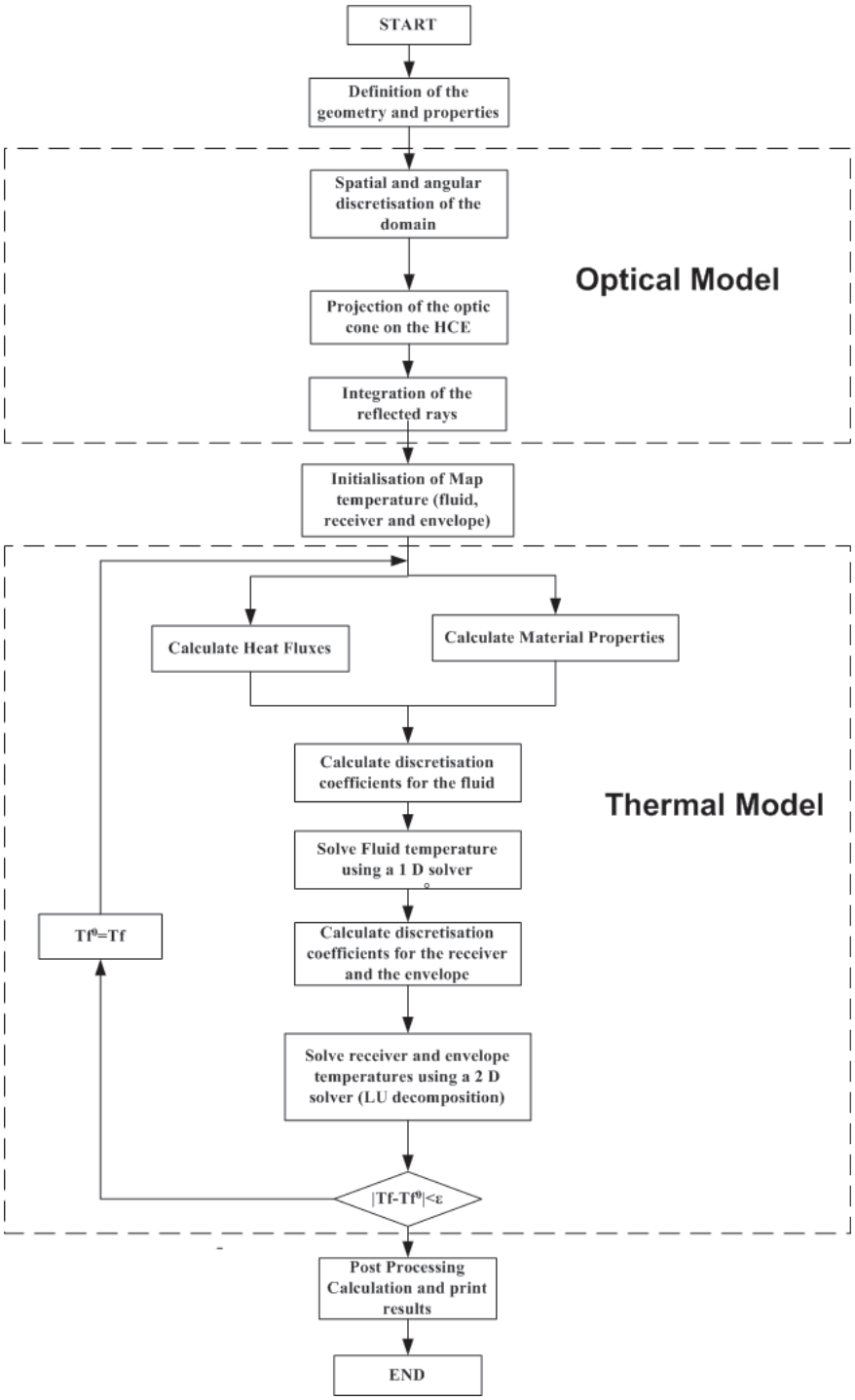

Figure 5: Flow chart of the general algorithm

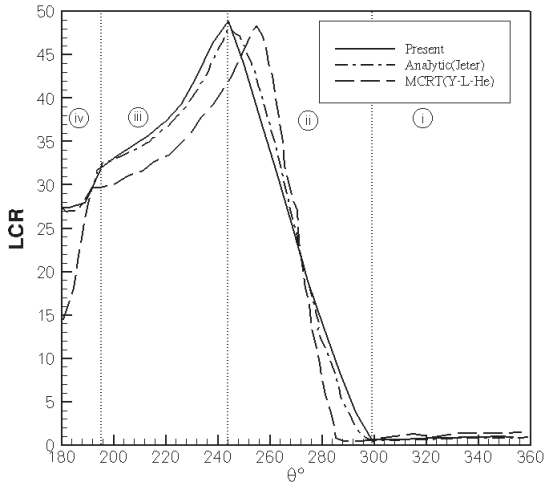

Figure 6: Local concentration ratio distribution along the azimuthal direction. Solid line: present results, dashed line: analytical results of Jeter [9], dashed-dotted line: MCRT results of He et al. [11]

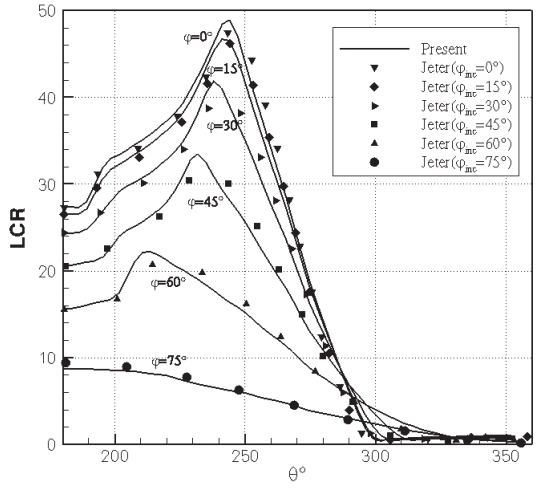

Figure 7: Local concentration ratio distribution along the azimuthal direction for different incident angles. Solid line: present results, dashed line: analytical results of Jeter [9]

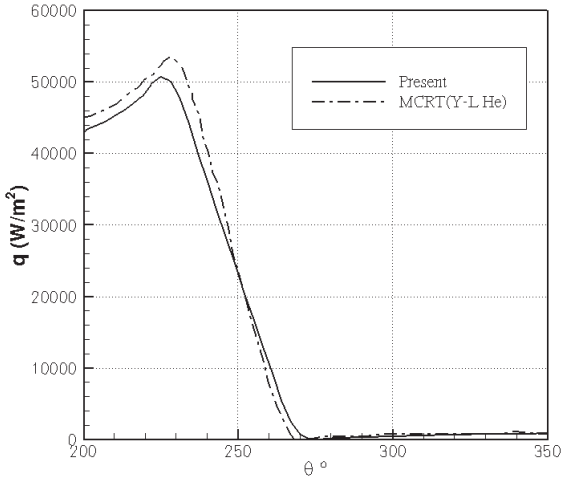

Figure 8: Heat flux distribution around the absorber tube for LS-2 collector with incident radiation of 933.7 W/m^2. Comparison with the results of He et al. [11].

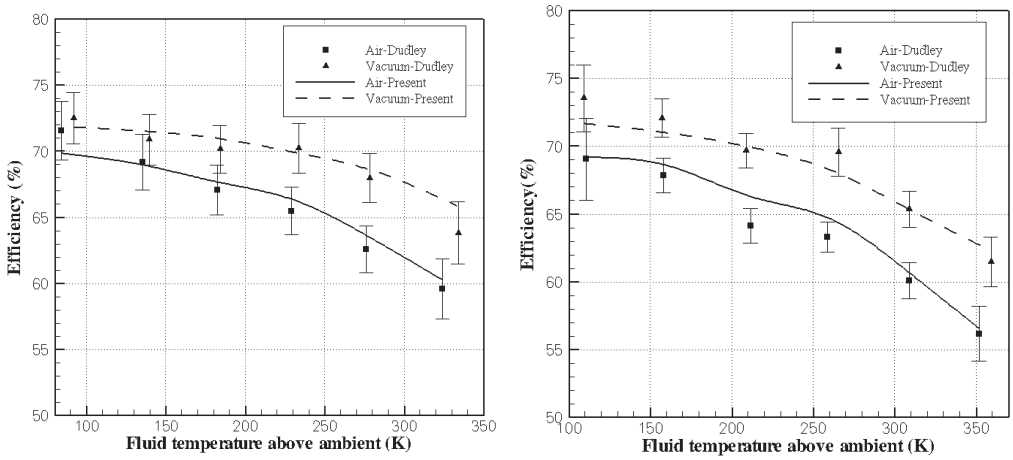

(a) (b)

Figure 9: Thermal efficiency comparison between Sandia experimental data and proposed model (a) cermet coating (b)black chrome coating

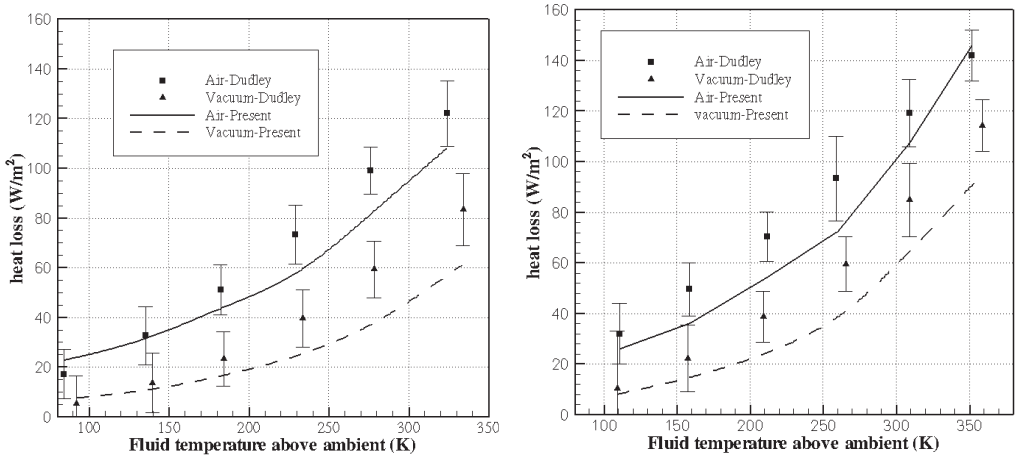

(a) (b)

Figure 10: Thermal losses comparison between Sandia experimental data and proposed model for irradiated case (a) cermet coating (b)black chrome coating

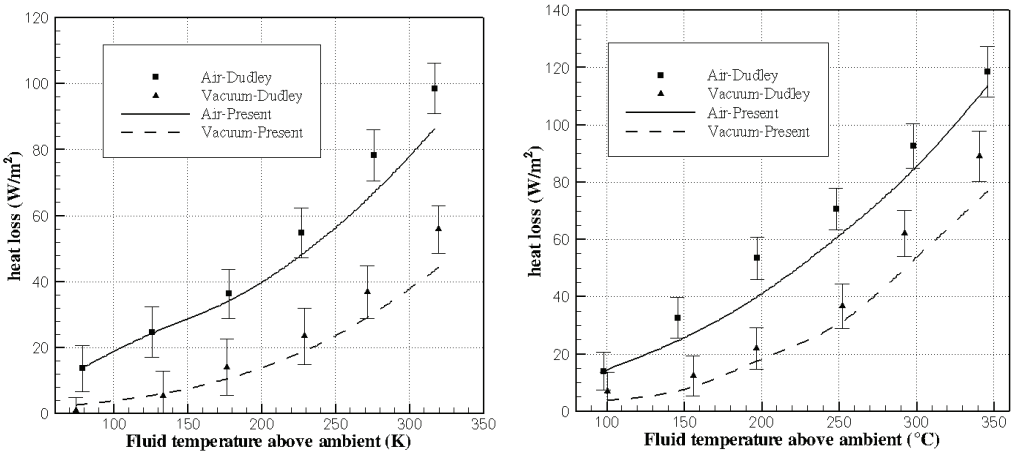

(a) (b)

Figure 11: Thermal losses comparison between Sandia experimental data and proposed model for un-irradiated case (a) cermet coating (b)black chrome coating

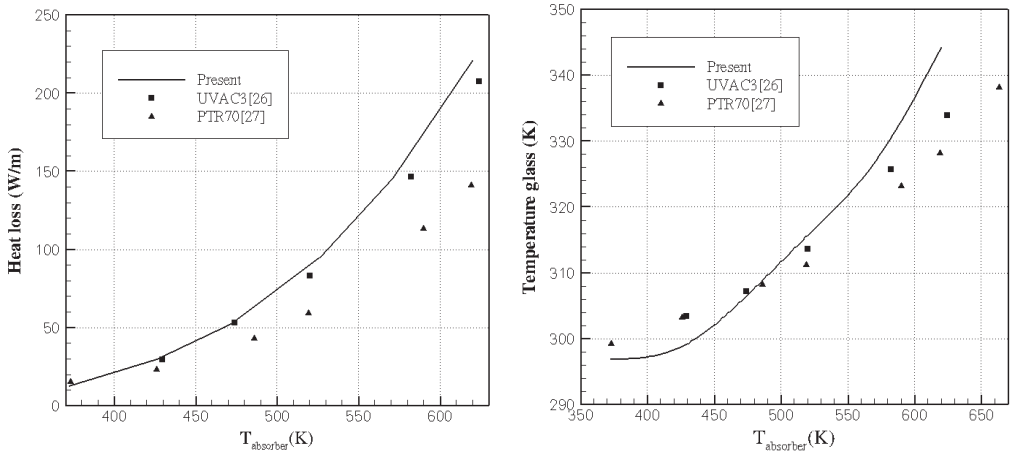

(a) (b)

Figure 12: Comparisons with un-irradiated absorbers experiments (a) heat losses and (b) glass temperature

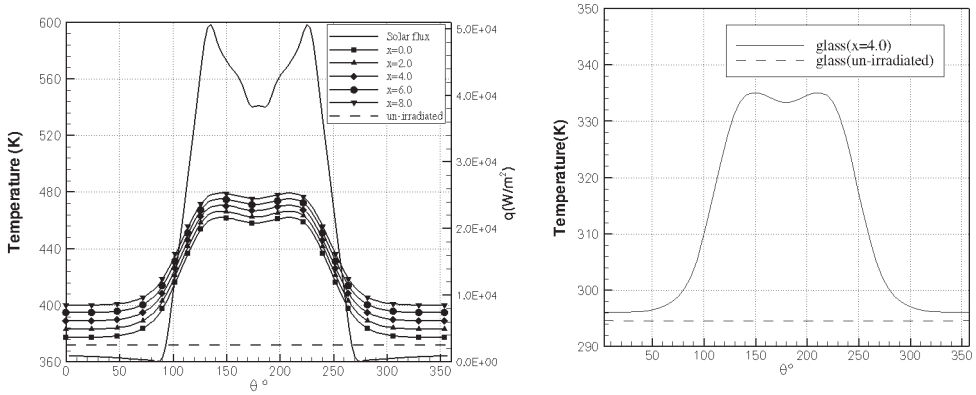

(a) (b)

Figure 13: Circumferential temperature distribution on (a) the absorber tube for several longitudinal positions (b) the glass cover for x=4.0m

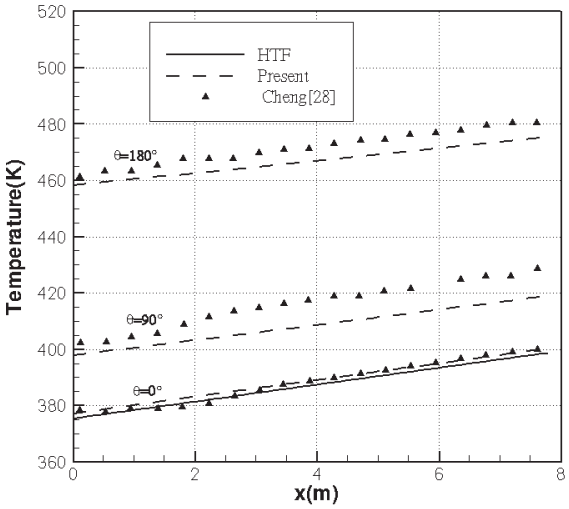

Figure 14: Variation of the temperature of the absorber tube and the HTF along the axial direction